

# Gold nanoparticles stabilized by modified halloysite nanotubes for catalytic applications

Marina Massaro,<sup>a,\*</sup> Carmelo G. Colletti,<sup>a</sup> Bruno Fiore,<sup>a</sup> Valeria La Parola,<sup>b</sup> Giuseppe Lazzara,<sup>c</sup>  
Susanna Guernelli,<sup>d</sup> Nelsi Zaccheroni<sup>d</sup> and Serena Riela<sup>a,\*</sup>

<sup>a</sup>Dipartimento STEBICEF, Sez. Chimica, Università degli Studi di Palermo, Viale delle Scienze, Ed. 17, 90128 Palermo, Italy. E-mails: [marina.massaro@unipa.it](mailto:marina.massaro@unipa.it); [serena.riela@unipa.it](mailto:serena.riela@unipa.it).

<sup>b</sup>Istituto per lo Studio dei Materiali Nanostrutturati ISMN-CNR, Via Ugo La Malfa 153, 90146 Palermo, Italy.

<sup>c</sup>Dipartimento di Fisica e Chimica, Università degli Studi di Palermo, Viale delle Scienze, Ed. 17, 90128 Palermo, Italy.

<sup>d</sup>Dipartimento di Chimica “G. Ciamician”, Università degli Studi di Bologna, Via S. Giacomo 11, 40126 Bologna, Italy.

KEYWORDS. Halloysite nanotubes, gold nanoparticles, reduction reactions, flow technology.

ABSTRACT. A highly sustainable prototype of a flow system based on gold nanoparticles (4.2 nm) supported on thiol functionalized HNT was developed for catalytic applications. The catalytic performances were evaluated by using the reduction of 4-nitrophenol to 4-aminophenol as model system. In the best experimental conditions (0.0001 mol%,  $1.97 \times 10^{-8}$  mg of AuNPs) impressive apparent turnover frequency (TOF<sub>a</sub>) value up to 2,204,530 h<sup>-1</sup> has been achieved and the halloysite based catalyst showed full recyclability even after ten cycles. The high catalytic activity confirms the importance of the use of HNT as support for AuNPs that can exert a synergistic effect both as medium for transfer of electron from borohydride ions to 4-NP and by modulating interfacial electron transfer dynamics. With the application of flow technology, the

obtained heterogeneous HNT@Au catalyst has been fully recovered and reused for at least one month.

INTRODUCTION. Halloysite nanotubes (HNTs), are an aluminosilicate clay with a predominantly hollow tubular structure, which have attracted a lot of interest due to their unique features, such as low toxicity, high specific surface area and natural availability at low price. HNTs consist in 10-15 aluminosilicate layers with an external surface constituted by siloxane groups and an inner lumen composed of aluminol groups.<sup>[1]</sup> Owing to this peculiar composition, HNTs are negatively charged on the external surface whereas they are positively charged in the inner one in a pH ranging from 2 to 8. The different surface chemistry allows the selective functionalization at the inner or outer side making possible the synthesis of several nanomaterials with appealing properties.<sup>[2]</sup> HNTs are no-toxic for a number of living organisms<sup>[3]</sup> and are widely used in many fields<sup>[4]</sup> such as filler for polymer<sup>[5]</sup> or hydrogel matrices,<sup>[6]</sup> drug carrier<sup>[7]</sup> and delivery,<sup>[8]</sup> adsorbent<sup>[9]</sup> as well as catalyst support.<sup>[10]</sup> In this context several metal catalysts loaded on the HNTs with excellent catalytic performances have been reported and reviewed.<sup>[2a, 10b, 11]</sup>

Among the plethora of metal nanoparticles, the gold ones (AuNPs), have gathered particular attention for applications in chemical synthesis since they show high thermal stability and excellent catalytic performances. However, the use AuNPs for industrial purposes is limited by their tendency to agglomerate forming clusters which lead to a loss of the catalytic activity. To overcome this drawback AuNPs can be anchored to solid supports. In this regard, gold nanoparticles were successfully loaded on pristine halloysite<sup>[12]</sup> and the obtained Au/HNTs hybrid showed high catalytic activity for solvent-free oxidation of benzyl alcohol.<sup>[13]</sup>

To best of our knowledge, very few papers reported the immobilization of gold nanoparticles on functionalized halloysite and all of these consider the formation of metal NPs by calcination methods.<sup>[14]</sup>

Herein, we report the synthesis and characterization of novel nanocatalyst based on halloysite and gold nanoparticles (HNT@Au) by chemical reduction. The new material is thoroughly investigated by means of several techniques. To evaluate the feasibility of the hybrid as catalyst, we studied the reduction of 4-nitrophenol at different NaBH<sub>4</sub> and catalyst concentration as model reaction. We also performed some recycling test to assess the stability of the material obtained. Finally, to define a practical and effective protocol to exploit the features of the solid catalytic system and to reach the highest level of sustainability, we propose a practical application of the system for industrial purposes taking advantages of flow chemistry.

**EXPERIMENTAL SECTION.** All reagents needed for the synthesis of HNT@Au nanocatalyst were purchased from Sigma-Aldrich and used without further purification. Halloysite nanotubes used in this study are from Sigma Aldrich. Microwave-assisted syntheses were carried out with a CEM DISCOVER monomode system in a closed vessel.  $\zeta$ -potential and dynamic light scattering (DLS) measurements were taken by using ZETASIZER NANO ZS90 (Malvern Instruments) at  $25.0 \pm 0.1$  °C. UV-vis measurements were performed using a Beckmann DU 650 spectrometer. Inductively Coupled Plasma-Optical Emission Spectrometry (ICP-OES) analyses were carried out with an Optima 2100, Perkin Elmer, equipped with an auto sampler model AS-90. Analyses were conducted using a calibration curve, obtained by dilution (range: 0–10 ppm) of palladium standard solution for ICP-OES analyses. The operative wavelengths were 340.458 and 363.470 nm. A scanning electron microscope (SEM—EVO50EP Carl Zeiss AG, Jena, Germany) was

used to obtain photomicrographs of the samples. The nanotubes were observed with carbon coating working in high vacuum at 20kV of accelerating voltage.

The EDS (Energy Dispersion Spectrometry) spectra were taken using an Oxford INCA 350 system showing the main elemental composition of the area itself. For TEM observation the samples were prepared using a drop of suspension on formvar-coated copper grid (400 mesh) and allowing the drop to dry completely in a vacuum desiccator. The TEM images of the samples were obtained using a Philips TEM CM 100 transmission electron microscope at accelerating voltage = 80 kV. X-ray diffraction (XRD) analyses were performed with a Bruker goniometer using Ni-filtered Cu K $\alpha$  radiation. A proportional counter and 0.05° step size in 2 $\theta$  were used. The assignment of the crystalline phases was based on the JPDS powder diffraction file cards. The X-ray photoelectron spectroscopy (XPS) analyses were performed with a VG Microtech ESCA 3000 Multilab, equipped with a dual Mg/Al anode. As excitation source was used the unmonochromatized Al K $\alpha$  radiation (1486.6 eV). The sample powders were analyzed mounted on a double-sided adhesive carbon tape. The pressure in the analysis chamber was in the range of 10<sup>-8</sup> Torr during data collection. The constant charging of the samples was removed by referencing all the energies to the Si 2p set at 103.8 eV, as internal standard. Analyses of the peaks were performed with the software CasaXPS. Atomic concentrations were calculated from peak intensity using the sensitivity factors provided with the software. The binding energy values are quoted with a precision of  $\pm 0.15$  eV and the atomic percentage with a precision of  $\pm 10\%$ .

The HNT-SH nanomaterial was prepared as previously reported.<sup>[15]</sup>

**Preparation of HNT@Au hybrid.** In a 10 mL round bottom flask were placed HNT-SH (0.25 g), HAuCl<sub>4</sub>×3H<sub>2</sub>O (0.05 g, 0.13 mmol) and water (4 mL). The obtained dispersion was stirred for 18 h at room temperature. The mixture was filtered under reduced pressure, washed with

water and dried under reduced pressure at room temperature. The material was re-suspended in MeOH (4 mL) and to this dispersion NaBH<sub>4</sub> (0.03 g, 0.8 mmol), as a reducing agent, was added. The suspension was stirred at room temperature for 18 h. The dispersion was filtered under reduced pressure, washed several times with MeOH and then dried overnight under reduced pressure at 60 °C.

**General conditions for the reduction nitroarenes.** Generally, HNT@Au aqueous suspension (different volume to reach the desired catalyst amount) was added into a mixed aqueous solution of 2 mL containing a nitroarene (0.10 mM) and NaBH<sub>4</sub> (from 8 to 50 mM) in a quartz cuvette, at room temperature and under stirring. The reduction process was monitored by recording the UV-vis spectra of the reaction mixture at 2 min intervals during the reaction. The reaction rate constant was determined by measuring the absorbance intensity of the initially observed peak of the substrate, as a function of time.

**Recyclability of the catalyst.** HNT-SH/Au catalyst (5 mg), 4-nitrophenol (0.3 mM), and NaBH<sub>4</sub> (33 mM) were placed in a vial under constant stirring and at room temperature. After 30 min, the complete reduction was checked by measuring the absorbance intensity at 397 nm. The reaction mixture was then centrifuged and the supernatant was decanted; the residual solid was washed three times with water, the HNT@Au catalyst was dried and reused in the same reaction for ten consecutive cycles.

**Reduction of 4-NP under flow conditions.** A glass tube column with an inner diameter of 10 mm and a length of 100 mm (Supelco Omnifit Column Kit) was filled with sand (50-70 mesh) and 1 wt% of HNT@Au catalyst (pore volume 1.26-1.34 mL g<sup>-1</sup>). The column was first eluted with water by using a peristaltic pump (LC-10AD VP Shimadzu). For evaluate the catalytic performance of the system, a mixed solution of 4-NP (0.100 mM) and NaBH<sub>4</sub> (100 mM) was

charged in a round bottom flask functioning as a reservoir. The equipment was connected, by using the appropriate tubes and valves, to the pump and installed into a thermostated box. The reaction mixture was cyclically pumped (flow rate 4.0 mL/min) through the catalyst column at 25 °C until complete conversion of the reactant was achieved (reaction was monitored by Uv-vis). To clean the reactor, water was cyclically pumped through the catalyst column for 15 min.

## RESULTS AND DISCUSSION

Since thiols are widely employed as an anchoring group for gold nanoparticles due to the strong Au-thiol bond,<sup>[16]</sup> the first step for the synthesis of the gold nanoparticles supported on HNT (HNT@Au) was the modification of the halloysite nanotubes with thiol-terminated organosilane following a procedure reported elsewhere.<sup>[10a]</sup> In particular, the condensation reaction between the organosilane and the hydroxyl groups present on the HNTs surface was carried out in solvent-free conditions, under microwave irradiations (Scheme 1). After the work up, the degree of functionalization of halloysite, estimated by TGA, was 0.4 mmol g<sup>-1</sup>. In the second step the immobilization of gold nanoparticles on thiol functionalized halloysite (HNT-SH) was carried out in an aqueous medium at room temperature. The formation of the AuNPs was achieved by adding an aqueous solution of HAuCl<sub>4</sub> to an aqueous dispersion of HNT-SH, followed by reduction with NaBH<sub>4</sub> in methanol. During the reduction reaction, the solution color changes from yellow to brown. The dispersion was then filtered to remove the supernatant solution, and finally it was dried under vacuum. In the same experimental conditions, pristine HNT did not interact with AuNPs.

### Scheme 1.

The content of gold nanoparticles, on the solid halloysite support, was determined by Inductively Coupled Plasma-Optical Emission Spectrometry (ICP-OES) and was estimated a total gold amount of 6.6 wt%. As shown in the energy-disperse X-ray (EDS) pattern, the weak but evenly distributed signals from Au further confirmed the presence of gold nanoparticles in the sample (Figure 1a). Furthermore, EDS measurements confirmed the successful functionalization highlighting the presence of sulfur in the structure of the nanomaterial deriving from the covalently grafted organosilane. SEM micrographs (Figure 1b) showed that the characteristic lengths and the tubular shape of HNTs were preserved in the HNT@Au catalyst. It should be noted that flake-like particles are imaged by SEM (figure 1b) that corresponds to the kaolinite typically presents in HNTs sample.

#### **Figure 1.**

The morphology of HNT@Au nanomaterial was investigated by TEM microscopy. The gold nanoparticles presented a spherical shape and were found to be mainly attached on the support surface. The HNT@Au material showed quite a uniform distribution of AuNPs with an average diameter of  $4.2 \pm 1.5$  nm (Figure 2), thus the gold nanoparticles are distributed on halloysite surface without negligible aggregation.

#### **Figure 2.**

The HNT@Au nanomaterial was further characterized by XRD and XPS analyses.

XRD spectra of HNT and HNT@Au are shown in Figure 3a. The pattern of HNT (black line) is typical of halloysite<sup>[17]</sup> with some crystallized quartz.<sup>[18]</sup> Upon functionalization, the XRD pattern (not shown) remain unchanged, indicating that no structural modification occurs. The

HNT@Au sample shows, besides the HNT structure, the presence of peaks at 38.2, 44.4 and 64.7  $2\theta$  typical of the cubic structure of gold particles.<sup>[19]</sup>

XPS data are summarized in Table 1. Binding energy of Si2p and Al2p emission occurs at 103.8 and 75.5 eV respectively and are typical of HNT materials. Position does not change after functionalization indicating that no electronic modifications occur. Moreover, all samples show a Si/Al atomic ratio higher than 1 which is in accordance with the structure of halloysite consisting of hollow cylinders formed by multiple-rolled layers containing gibbsite octahedral sheet (Al-OH) groups on the internal surface and siloxane groups (Si-O-Si) on the external surface.

The thiol functionalization of the HNT is confirmed by the appearance of the S2p peak at 164.1 eV which is typical of thiolic sulphur<sup>[20]</sup> (Figure S1). The intensity of this peak decrease drastically in HNT@Au because AuNP grows on the SH termination and covers totally the sulphur atoms. Au4f7/2 binding energy is centered at 85.0 eV. This value is slightly higher than metallic gold (usually at 84.0 eV) and is attributed to slightly positive surface gold atoms that are chemically bonded to the thiol moieties.<sup>[21]</sup>

**Table 1.**

**Figure 3.**

**Catalytic Activity of HNT@Au nanomaterial.**

To evaluate the catalytic performance of the HNT@Au hybrid nanomaterial obtained, we chose the reduction of 4-nitrophenol (4-NP) by NaBH<sub>4</sub> that is the most used reaction to test the catalytic activity of metal nanoparticles in aqueous solution.<sup>[22]</sup> The interest in this reaction is mainly due to the fact that 4-NP is a common reactant in pharmaceuticals and can be a hazardous by-product that is inhibitory and toxic in nature, whereas 4-aminophenol (4-AP) is used for black-and-white films and for the production of acetaminophen.



The NaBH<sub>4</sub> mediated reduction of 4-NP is thermodynamically feasible (since E<sub>0</sub> for 4-NP/4-AP is -0.76 V and for H<sub>3</sub>BO<sub>3</sub>/BH<sub>4</sub><sup>-</sup> -1.33 V vs NHE) but kinetically restricted due to the large potential difference between donor (BH<sub>4</sub><sup>-</sup>) and acceptor (4-NP) species with decreases the feasibility of this reaction. The gold nanoparticles, with the suitable redox potential help to overcome the kinetic barrier by facilitating relay of electrons from donor to acceptor species.<sup>[23]</sup> Furthermore, this reaction can be easily monitored by UV-vis spectroscopy.

The aqueous solution of 4-NP is pale yellow and it changes into yellow-green with the addition of NaBH<sub>4</sub> due to the formation of 4-nitrophenolate ions; as a consequence, the maximum absorption peak of 4-NP aqueous solution centered at 317 nm shifted to 396 nm after the addition of NaBH<sub>4</sub>. First of all, the reduction reaction was followed in absence of Au nanoparticles. By adding the HNT-SH nanomaterial in the reaction mixture the intensity of the absorbance remained unchanged at 396 nm even after several days, which revealed that no reduction of 4-NP occurred (Figure S2). On the contrary, with the addition of the catalytic nanomaterial HNT@Au, the solution color faded from yellow-green to transparent with time and the reduction reaction comes to completeness within 7 min. We investigated the influence of NaBH<sub>4</sub> concentration on the reduction reaction. The typical time dependent UV-vis spectra of 4-NP reduction are shown in Figure 4. At low NaBH<sub>4</sub> concentration, e.g., 9 mM, we observed a slow decrease in the absorbance intensity at 396 nm as a function of reaction time with the concomitant appearance of a peak at 300 nm, corresponding to the characteristic absorption of 4-AP. The reducing reaction is rather slow and only 30% of 4-NP was reduced after 1 h (Figure 4a). On the other hand, the increasing of NaBH<sub>4</sub> (25 mM) concentration led to an increase in the reaction rate and the 4-NP was completely reduced after only 6 min (Figure 4b).

The reaction kinetics can be analyzed by plotting the absorbance value at 396 nm as a function of time. Figure 5 shows the plot of  $\ln(A_t/A_0)$  vs reaction time, where  $A_t$  is the absorbance at reaction time  $t$  and  $A_0$  is the initial absorbance. The results indicate that  $\ln(A_t/A_0)$  decreases linearly with reaction time, which is consistent with the pseudo-first-order kinetics of 4-NP reduction by  $\text{NaBH}_4$ .<sup>[24]</sup> The apparent reaction time constant  $k_{app}$  ( $\text{s}^{-1}$ ) was estimated by the linear fitting of the experimental results and the obtained data are listed in Table S1. The actual kinetic constant ( $k$ ) can be easily determined by the slope of the plot  $k_{app}$  versus  $[\text{NaBH}_4]$ .

**Figure 4.**

**Figure 5.**

Since the reduction of 4-NP is strictly depended on the amount of AuNPs introduced in the system we performed an additional study varying the amount of the catalyst (Table 2). To further estimate the catalytic efficiency of the new hybrid obtained we calculated the apparent turnover frequency ( $\text{TOF}_a$ ) values.<sup>[25]</sup> The obtained results are reported in Table 2.

Surprisingly, in this case an increase of the catalyst amount led to a decrease in the reaction rate (Figure 4a, Table 2, entry 1).

**Table 2.**

To deep investigate the catalytic process and to understand this apparently anomalous behavior the colloidal stability of the catalyst in water was investigated by  $\zeta$ -potential and dynamic light scattering (DLS).  $\zeta$ -potential data clearly show that, as expected, the  $-\text{SH}$  surface functionalization of HNT did not alter the surface charge of the nanotubes (Table 3). On the other hand, the HNT@Au hybrid system showed a change in the  $\zeta$ -potential in the direction of a reduction of negative site at the outer HNT surface (Table 3). This effect agrees with the Au

linkage to –SH moiety and indicates that the HNT@Au system presents a reduction of its colloidal stability due to limited electrostatic repulsions.

**Table 3.**

The hydrodynamic radius obtained by DLS experiments provided a clear understanding of the aggregation behavior of the nanoparticles in water as a function of their concentration. Figure 6 shows the trend of the apparent hydrodynamic radius with the catalyst concentration in water. In the dilute regime, the obtained size corresponds to that of HNT-SH (dotted line in Figure 6) as the nanomaterial does not undergo to aggregation in the solvent media. Increasing the concentration generates a larger apparent hydrodynamic radius that indicates aggregation between particles with a consequent reduction of the active surface available for the catalytic process. In other words, due to aggregation one obtains greater particles size and therefore the catalytic active sites accessible to the reactants are reduced and generated worse catalytic performances.

**Figure 6.**

To the light of the above results we tried to further improve the catalytic performance of the HNT@Au hybrid. In particular, we performed some additional catalytic tests increasing the amount of NaBH<sub>4</sub> to 50 mM and varying the catalyst amount from 0.01 to 0.0001 mol%. The obtained results are collected in Figure 5b and Table 4. The data confirm the DLS results; indeed, in an aqueous dilute regime, no aggregation of nanoparticles was observed and the reaction rate depends only on the amount of catalyst.

**Table 4.**

As it is possible to observe from Figure 5b, when the amount of catalyst is very low, there is no change in the absorbance of 4-NP within the first seconds, and therefore the reaction proceeds

with an initial induction period ( $t_0$ ). During this period, the HNT@Au hybrid does not seem to participate in the reduction reaction, and the catalysis reaction is paralyzed until the induction period is finished.<sup>[26]</sup> After this  $t_0$ , the reduction starts and the absorbance of 4-NP decreases at a fast speed. This induction period is normally observed in most of the catalytic reductions involving 4-NP and it is related to the diffusion time required for the adsorption of the reactants onto the catalyst surfaces before initiation of the reaction. At higher catalyst concentration, probably the adsorption of the 4-NP on the halloysite surface was fast and no induction period is observed. When the catalyst concentration is low, the adsorption of 4-NP needs more time, since less active sites were available and we observed an induction period of several seconds.

When catalyst loading was further decreased down to 0.001 mol%, the 4-NP was successfully reduced to 4-aminophenol in a few minutes (entry 2) with an apparent turnover frequency (TOF<sub>a</sub>) of 186,340 h<sup>-1</sup>. Further improvement has been obtained by decreasing the amount of gold nanoparticles. Just 0.0001 mol% of HNT@Au ( $1.97 \times 10^{-8}$  mg of AuNPs) is sufficient to quantitatively yield the amino derivative in *ca.* 27 min with a  $k_{app}$  value of 0.0018 s<sup>-1</sup> (entry 3). In such a way, a remarkable TOF<sub>a</sub> value of 2,204,530 h<sup>-1</sup> was achieved. To the best of our knowledge, this value is the highest reported for AuNPs immobilized on a solid support (Table 5).

#### **Table 5.**

To study the recyclability of the HNT@Au hybrid nanocomposites, the same catalyst was used to perform the same reduction reaction for the consecutive runs. After each catalytic cycle, the catalyst (5 mg) was centrifuged, washed several times with water and dried for the next cycle of catalysis. The catalyst exhibits high activity in the same reaction time (30 min) after running for 10 cycles without presumably leaching of gold nanoparticles (Figure S3). Such results indicate that the presence of thiol functionalized halloysite as support for gold, was sufficient to stabilize

the catalytic nanoparticles by preventing their aggregation, producing a good catalyst with high activity and stability.

### **Proposed reaction mechanism**

These interesting results could be explained by a synergistic effect between halloysite and AuNPs in the hybrid nanomaterial. In fact, the hollow nanotubular structure of halloysite with high specific surface area and considerable adsorption ability, promotes the diffusion of the reactants and the adsorption rate. Besides, the surface chemical structures of rolling silica tetrahedral layers and alumina octahedral layers with a higher conduction band edge in halloysite, may modulate interfacial electron transfer dynamics. Based on these evidences, we proposed a reaction mechanism as follows.

Halloysite could significantly attract the negatively charged nitrophenolate ions into positively charged lumen through both electrostatic and hydrophobic interaction, resulting in their enrichment on HNT@Au surface. Then  $\text{BH}_4^-$  ions transfer electrons to the catalyst surface which acts as medium for transfer of electron from borohydride ions to 4-NP. Therefore, electrons leave the gold nanoparticles and end up with an electron enriched region at the interface of gold nanoparticles and halloysite support. The existence of the surplus electrons added to the HNT surface facilitates the uptake of electrons by the adsorbed 4-nitrophenol molecules, which leads to the reduction of 4-nitrophenol into the 4-aminophenol (Figure 7).

### **Figure 7.**

### **Screening of different substrates**

Hence, the applicability of the reaction has been checked on a set of nitroarene derivatives (Figure S4) having either electron-donating or electron-withdrawing groups in different positions

respect to the nitro group (Table 6). To achieve this scope, we choose to run the reactions in the presence of 0.1 mol% of catalyst with 50 mM of NaBH<sub>4</sub> to clearly monitor the conversion efficiency of the reaction. It seems clearly that the presence of a strong electron donating substituent at the para position with respect to the reacting nitro group, is an important requirement for the reaction to occur (entries 1, 4, 5, 6). In particular, 4-nitroaniline (entry 1) and 4-(4-nitrophenyl)morpholine (entry 6) are more reactive than other nitroaniline derivatives, while the methyl 2-((4-nitrophenyl)amino)acetate (entry 8) is not reactive at all. The presence of substituent in meta or ortho position with respect to nitro group significantly reduces the reaction rate.

The N-substituted derivative (entry 7) shows less reactivity than the correspondent nitroaniline compound (entry 4), despite alkyl substituents on the N atom should enhance the overall electron donating character of the group. Furthermore, it was observed that the presence of a negative charge on the ancillary chain bound to the N atom (entries 4 and 7), disadvantages the reduction reaction. This probably reflects a more difficult approach of the anionic reducing agent to the nitroarene-catalyst.<sup>[27]</sup>

### **Table 6.**

#### **Flow Chemistry approach**

We finally focused the attention on the use of flow technology as an alternative efficient stirring method able to preserve the efficiency of a heterogeneous catalytic system, simplify its recovery and reuse.<sup>[28]</sup>

In particular, the reduction reaction takes place inside a glass tube column using a mixture of sand impregnated with 1 wt% of the HNT@Au catalyst, as stationary phase and the reactants solution was charged in a reservoir (Figure 8). Sand was added as inert support to both improve

the flowability of the overall system and minimize the amount of catalyst in the column. The column was connected, by using the appropriate tubes and valves, to a peristaltic pump and installed into a thermostated box. After setting the temperature to 25 °C the reaction mixture was cyclically pumped through the column at a 4.0 mL/min flow rate for 90 min, time required to obtain quantitative conversion.

After each catalytic cycle the column containing the catalyst was cyclically washed with water to remove any residues. After this treatment, a second batch of reactants was charged in the reservoir, and quantitative conversion to product was achieved again. The reuse of the catalyst was repeated for at least three representative runs. With the final goal to obtain a greener process the amount of NaBH<sub>4</sub> was decreased from 25 to 5 mM; in the last case total conversion was obtained after 120 min.

### **Figure 8.**

## CONCLUSIONS

A prototype of a flow system based on gold nanoparticles supported on thiol functionalized HNT for the reduction of 4-NP to 4-AP was developed.

The catalytic performance of the HNT@Au nanomaterial was tested in the reduction reaction by varying the NaBH<sub>4</sub> and catalyst concentrations. The collected data show that the apparent kinetic constant increases with increasing of NaBH<sub>4</sub> concentration, on the contrary, surprisingly, it decreases with increasing the amount of the catalyst. DLS measurements highlighted that at higher catalyst concentrations, aggregation between nanoparticles occurs and greater particles size are observed. Consequently, the catalytic active sites accessible to the reactants are reduced

and worse catalytic performances are obtained. In an aqueous dilute regime, no aggregation of nanoparticles was observed and the reaction rate depends only on the amount of catalyst.

The applicability of the reaction has been checked on a set of nitroarene derivatives showing that the reaction is promoted by the presence of electron donating group in para position with respect to the reaction center. The catalyst was used without loss in its catalytic activity for at least ten cycles.

The catalytic performances of HNT@Au were outstanding, reaching remarkable TOF values (up to 2,204,530 h<sup>-1</sup>). To the best of our knowledge, this value probably represents the highest value ever reported for the reduction of 4-NP by AuNPs immobilized on a solid support.

Finally, the flow approach adopted is an efficient technological solution to preserve the physical integrity of the catalyst and also to allow for its easy recovery and recycle.

#### ACKNOWLEDGMENT

The work was financially supported by the University of Palermo. The authors would thanks Dr A. Pettignano (University of Palermo) for ICP-OES analyses and Prof. P. Lo Meo (University of Palermo) for providing some nitroarene derivatives.

#### REFERENCES

- [1] a) Y. Lvov, W. Wang, L. Zhang, R. Fakhrullin, *Adv. Mater.* **2016**, *28*, 1227; b) G. Cavallaro, G. Lazzara, S. Milioto, *Langmuir* **2011**, *27*, 1158.
- [2] a) M. Massaro, C. G. Colletti, G. Lazzara, S. Milioto, R. Noto, S. Riela, *J. Mater. Chem. A* **2017**, *5*, 13276; b) M. Massaro, G. Lazzara, S. Milioto, R. Noto, S. Riela, *J. Mater. Chem. B* **2017**, *5*, 2867.
- [3] a) G. I. Fakhrullina, F. S. Akhatova, Y. M. Lvov, R. F. Fakhrullin, *Environ. Sci.: Nano* **2015**, *2*, 54; b) T. G. Shutava, R. F. Fakhrullin, Y. M. Lvov, *Curr. Opin. Pharmacol.* **2014**, *18*, 141; c) L. Bellani, L. Giorgetti, S. Riela, G. Lazzara, A. Scialabba, M. Massaro, *Environ. Toxicol. Chem.* **2016**, *35*, 2503.
- [4] a) Y. Fu, D. Zhao, P. Yao, W. Wang, L. Zhang, Y. Lvov, *ACS Appl. Mater. Inter.* **2015**, *7*, 8156; b) E. A. Naumenko, I. D. Guryanov, R. Yendluri, Y. M. Lvov, R. F. Fakhrullin, *Nanoscale* **2016**, *8*, 7257; c) J. Tully, R. Yendluri, Y. Lvov, *Biomacromolecules* **2016**, *17*, 615.



- [5] a) M. Liu, Z. Jia, F. Liu, D. Jia, B. Guo, *J. Colloid Interf. Sci.* **2010**, *350*, 186; b) R. T. D. Silva, P. Pooria, K. L. Goh, S. P. Chai, J. Chen, *J. Compos. Mater.* **2013**, *48*, 3705; c) A. Sorrentino, G. Gorrasi, V. Vittoria, *Trends Food Sci. Tech.* **2007**, *18*, 84.
- [6] a) L. Fan, J. Zhang, A. Wang, *J. Mater. Chem. B* **2013**, *1*, 6261; b) C. Rizzo, R. Arrigo, F. D'Anna, F. Di Blasi, N. T. Dintcheva, G. Lazzara, F. Parisi, S. Riela, G. Spinelli, M. Massaro, *J. Mater. Chem. B* **2017**, *5*, 3217.
- [7] a) M. Liu, Y. Chang, J. Yang, Y. You, R. He, T. Chen, C. Zhou, *J. Mater. Chem. B* **2016**, *4*, 2253; b) M. Massaro, G. Cavallaro, C. G. Colletti, G. D'Azzo, S. Guernelli, G. Lazzara, S. Pieraccini, S. Riela, *J. Colloid Interface Sci.* **2018**, *524*, 156.
- [8] M. Massaro, S. Riela, C. Baiamonte, J. L. J. Blanco, C. Giordano, P. Lo Meo, S. Milioto, R. Noto, F. Parisi, G. Pizzolanti, G. Lazzara, *RSC Adv.* **2016**, *6*, 87935.
- [9] a) Q. Peng, M. Liu, J. Zheng, C. Zhou, *Micropor. Mesopor. Mat.* **2015**, *201*, 190; b) M. Massaro, C. G. Colletti, G. Lazzara, S. Guernelli, R. Noto, S. Riela, *ACS Sustain. Chem. Eng.* **2017**, *5*, 3346; c) S. Cataldo, G. Lazzara, M. Massaro, N. Muratore, A. Pettignano, S. Riela, *Appl. Clay Sci.* **2018**, *156*, 87.
- [10] a) M. Massaro, V. Schembri, V. Campisciano, G. Cavallaro, G. Lazzara, S. Milioto, R. Noto, F. Parisi, S. Riela, *RSC Adv.* **2016**, *6*, 55312; b) M. Massaro, S. Riela, G. Cavallaro, C. G. Colletti, S. Milioto, R. Noto, F. Parisi, G. Lazzara, *J. Molecul. Catal. A* **2015**, *408*, 12; c) M. Massaro, S. Riela, G. Lazzara, M. Gruttadauria, S. Milioto, R. Noto, *Appl. Organomet. Chem.* **2014**, *28*, 234.
- [11] a) G. S. Machado, O. J. d. Lima, K. J. Ciuffi, F. Wypych, S. Nakagaki, *Catal. Sci. Tech.* **2013**, *3*, 1094; b) A. M. Carrillo, J. G. Carriazo, *Appl. Catal., B* **2015**, *164*, 443; c) C. Li, X. Li, X. Duan, G. Li, J. Wang, *J. Colloid Interface Sci.* **2014**, *436*, 70; d) Y. Zhang, Y. Xie, A. Tang, Y. Zhou, J. Ouyang, H. Yang, *Ind. Eng. Chem. Res.* **2014**, *53*, 5507; e) Y. Zhang, A. Tang, H. Yang, J. Ouyang, *Appl. Clay Sci.* **2016**, *119*, 8; f) Y. Zhang, X. He, J. Ouyang, H. Yang, *Sci. Rep.* **2013**, *3*, 2948.
- [12] M. Zieba, J. L. Hueso, M. Arruebo, G. Martinez, J. Santamaria, *New J. Chem.* **2014**, *38*, 2037.
- [13] X. Fu, Z. Ding, X. Zhang, W. Weng, Y. Xu, J. Liao, Z. Xie, *Nanoscale Res. Lett.* **2014**, *9*, 282.
- [14] A. Philip, J. Lihavainen, M. Keinänen, T. T. Pakkanen, *Appl. Clay Sci.* **2017**, *143*, 80.
- [15] M. Massaro, S. Riela, G. Cavallaro, M. Gruttadauria, S. Milioto, R. Noto, G. Lazzara, *J. Organomet. Chem.* **2014**, *749*, 410.
- [16] S. M. Ansar, R. Haputhanthri, B. Edmonds, D. Liu, L. Yu, A. Sygula, D. Zhang, *J. Phys. Chem. C* **2011**, *115*, 653.
- [17] Z. MeiLing, D. MingLiang, Z. Han, X. CongSheng, F. YaQin, *J. Phys. D: Appl. Phys.* **2012**, *45*, 325302.
- [18] X. Wu, C. Liu, H. Qi, X. Zhang, J. Dai, Q. Zhang, L. Zhang, Y. Wu, X. Peng, *Appl. Clay Sci.* **2016**, *119*, 284.
- [19] B. Deiminiat, G. H. Rounaghi, *Sens. Actuator B-Chem.* **2018**, *259*, 133.
- [20] Z. Zhang, T. Li, Y. Li, L. Yan, L. An, *Mater. Chem. Phys.* **2018**, *209*, 271.
- [21] L. Carlini, C. Fasolato, P. Postorino, I. Fratoddi, I. Venditti, G. Testa, C. Battocchio, *Colloids Surf. A* **2017**, *532*, 183.
- [22] Y.-T. Liao, J. E. Chen, Y. Isida, T. Yonezawa, W.-C. Chang, S. M. Alshehri, Y. Yamauchi, K. C. W. Wu, *ChemCatChem* **2016**, *8*, 502.
- [23] X. Zeng, Z. Sun, H. Wang, Q. Wang, Y. Yang, *Compos. Sci. Technol.* **2016**, *122*, 149.

- [24] M. Chen, H. Kang, Y. Gong, J. Guo, H. Zhang, R. Liu, *ACS Appl. Mater. Interf.* **2015**, *7*, 21717.
- [25] X. Wu, C. Lu, Z. Zhou, G. Yuan, R. Xiong, X. Zhang, *Environm. Sci. Nano* **2014**, *1*, 71.
- [26] a) X. Zhou, W. Xu, G. Liu, D. Panda, P. Chen, *J. Am. Chem. Soc.* **2010**, *132*, 138; b) S. Wunder, Y. Lu, M. Albrecht, M. Ballauff, *ACS Catal.* **2011**, *1*, 908.
- [27] M. Russo, F. Armetta, S. Riela, D. Chillura Martino, P. L. Meo, R. Noto, *J. Mol. Catal. A* **2015**, *408*, 250.
- [28] C. Petrucci, G. Strappaveccia, F. Giacalone, M. Gruttadauria, F. Pizzo, L. Vaccaro, *ACS Sustain. Chem. Eng.* **2014**, *2*, 2813.
- [29] W. Shen, Y. Qu, X. Pei, S. Li, S. You, J. Wang, Z. Zhang, J. Zhou, *J. Hazard. Mater.* **2017**, *321*, 299.
- [30] K. Kuroda, T. Ishida, M. Haruta, *J. Mol. Catal. A* **2009**, *298*, 7.
- [31] Y.-C. Chang, D.-H. Chen, *J. Hazard. Mater.* **2009**, *165*, 664.
- [32] H. Koga, E. Tokunaga, M. Hidaka, Y. Umemura, T. Saito, A. Isogai, T. Kitaoka, *Chem. Commun.* **2010**, *46*, 8567.
- [33] A. Herreros-López, C. Hadad, L. Yate, A. A. Alshatwi, N. Vicentini, T. Carofiglio, M. Prato, *Eur. J. Org. Chem.* **2016**, *2016*, 3186.
- [34] A. T. Miah, S. K. Bharadwaj, P. Saikia, *Powder Technol.* **2017**, *315*, 147.
- [35] I. K. Sen, K. Maity, S. S. Islam, *Carbohydr. Polym.* **2013**, *91*, 518.

## List of Figures:

**Scheme 1.** Schematic representation of the synthesis of HNT@Au nanomaterial.

**Figure 1.** (a) EDS pattern; (b) SEM images of the HNT@Au catalyst.

**Figure 2.** (a-b) TEM images of the HNT@Au nanocatalyst; (c) AuNPs size distribution (n = 308).

**Figure 3.** (a) XRD spectra of HNT (black line) and HNT@Au (red line); (b) Al2p, Au4f and Si2p XPS region of HNT, HNT-SH and HNT@Au. The inset shows a magnification of Au4f.

**Figure 4.** Time dependent UV–vis spectra of the reduction of 4-NP at NaBH<sub>4</sub> concentration of (a) 9 and (b) 25 mM. The concentrations of 4-NP and AuNPs were 0.050 mM and 1 ng/mL, respectively.

**Figure 5.** Plot of  $\ln(A/A_0)$  versus time at different nanocatalyst concentration. The concentrations of 4-NP and NaBH<sub>4</sub> were 0.050 mM and (a) 25 mM (b) 50 mM, respectively.

**Figure 6.** Trend of the apparent hydrodynamic radius with the HNT@Au catalyst concentration in water (the dotted line represents the apparent hydrodynamic radius of HNT-SH nanomaterial in the same conditions).

**Figure 7.** Cartoon representation of the catalytic mechanism proposed.

**Figure 8.** Schematic Flow Reactor for the 4-NP reduction.

**Table 1.** XPS data.

	<b>Si2p (eV)</b>	<b>Al2p (eV)</b>	<b>Au4f7/2 (eV)</b>	<b>S2p (eV)</b>	<b>Si/Al</b>	<b>Au/Si</b>	<b>S/Si</b>
HNT	103.8	75.5			1.2	-	-
HNT-SH	103.8	75.4		164.1	1.2	-	0.14
HNT@Au	103.8	75.7	85.2		1.2	0.02	-

**Table 2.** Reduction of 4-NP at different catalyst concentration.<sup>a</sup>

Entry	Au (mol%)	$k_{app}$ (s <sup>-1</sup> )	TOF <sub>a</sub> (h <sup>-1</sup> ) <sup>b</sup>
1	1.01	0.0016	125
2	0.11	0.0069	7,470
3	0.05	0.0068	12,740
4	0.01	0.0063	97,040

<sup>a</sup>Reaction conditions: 0.050 mM of 4-NP and 25 mM of NaBH<sub>4</sub>.

<sup>b</sup>TOF<sub>a</sub> =  $n_p/n_c \cdot t$ , where  $n_p$  and  $n_c$  are the moles of the product molecules and the catalyst during time  $t$ , respectively

**Table 3.**  $\zeta$ -potential and DLS data for the nanomaterials investigated at different concentrations.

	Catalyst (mol%)	Hydrodynamic radius (nm)	$\zeta$ -Potential (mV)
pristine HNT	/	240 <sup>[8]</sup>	-37.6±1.4
HNT-SH	/	175	-36.9±1.6
HNT@Au	0.001	210	-20.6±1.6
HNT@Au	0.01	185	-20.3±1.6
HNT@Au	0.1	310	-20.5±1.6
HNT@Au	1	395	-26±2

**Table 4.** Reduction of 4-NP at different catalyst concentration.<sup>a</sup>

Entry	Au (mol%)	$k_{app}$ (s <sup>-1</sup> )	TOF <sub>a</sub> (h <sup>-1</sup> )
1	0.01	0.0115	145,160
2	0.001	0.0048	186,340
3	0.0001	0.0018	2,204,530

<sup>a</sup>Reaction conditions: 0.050 mM of 4-NP and 50 mM of NaBH<sub>4</sub>.

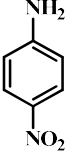
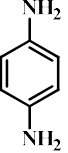
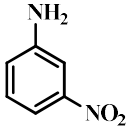
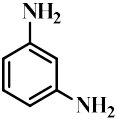
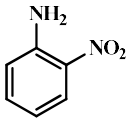
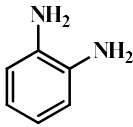
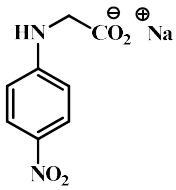
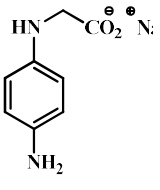
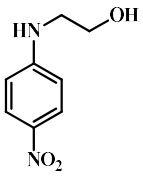
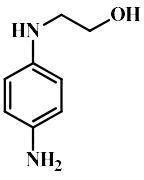
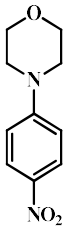
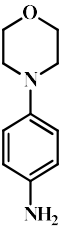
**Table 5.** Reduction of 4-NP over different Au nanocatalysts.

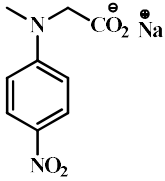
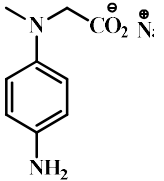
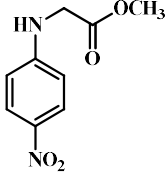
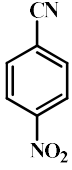
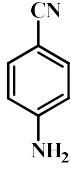
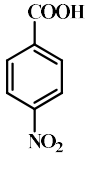
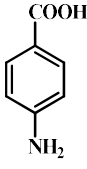
<b>Support</b>	<b>AuNPs size (nm)</b>	<b><math>k_{app}</math> (s<sup>-1</sup>)</b>	<b>TOF<sub>a</sub> (h<sup>-1</sup>)</b>	<b>Ref.</b>
AuNPs	4.4	$5.9 \times 10^{-1}$	115	[29]
PMMA	6.9	$7.2 \times 10^{-3}$	88.6	[30]
CNs	10-30	$2.1 \times 10^{-3}$	109	[25]
Chitosan	3.1	$1.2 \times 10^{-2}$	50.4	[31]
AOBC	10.6	$4.5 \times 10^{-3}$	1198	[24]
CSNFs	5	$5.9 \times 10^{-3}$	563	[32]
NCC-G <sup>AT</sup> <sub>0</sub>	3.5	$2.8 \times 10^{-3}$	608	[33]
SBA-15	2.3	$1.7 \times 10^{-2}$	a	[34]
NC	5.7	$3.6 \times 10^{-3}$	1185 <sup>b</sup>	[22]
Glucan	8	$1.9 \times 10^{-3}$	5922	[35]
HNT	4.2	$1.8 \times 10^{-3}$	2,204,530	this work

<sup>a</sup>No data available.<sup>b</sup>Calculated as the rate constant divided by the amount of gold on the support.



**Table 6.** Reduction of various nitroarenes using the HNT@Au catalyst under the optimized experimental conditions for 4-NP reduction.<sup>a</sup>

Entry	Substrate	Product	Time (min)	$k_{app}$ (s <sup>-1</sup> )	TOF <sub>a</sub> (h <sup>-1</sup> )
1			144	$4.2 \times 10^{-4}$	416
2			252	$1.0 \times 10^{-4}$	238
3			1175	$2.1 \times 10^{-5}$	54
4			600	$2.66 \times 10^{-5}$	100
5			638	$7.6 \times 10^{-5}$	86
6			223	$1.3 \times 10^{-4}$	270

7			240	$7.8 \times 10^{-5}$	124 <sup>b</sup>
8		No product	/	/	/
9			1000	$5.5 \times 10^{-5}$	71 <sup>c</sup>
10			540	$6.8 \times 10^{-5}$	29 <sup>b</sup>

<sup>a</sup>Reaction condition: nitroarene 0.1 mM, 0.1 mol% of HNT@Au catalyst 2  $\mu$ g of AuNPs), 0.50 mM of NaBH<sub>4</sub>.

<sup>b</sup>The absorbance value reaches a plateau after that the reaction does not continue.

<sup>c</sup>The reduction reaction was stopped after 1000 min.